Temperature dependence of electron density and electron-electron interactions in monolayer epitaxial graphene grown on SiC

Chieh-Wen Liu[1, 2, †], Chiashain Chuang[1, †], Yanfei Yang[1], Randolph E. Elmquist[1, *], Yi-Ju Ho[2], Hsin-Yen Lee[3], and Chi-Te Liang[2, 3, *]

[1]*National Institute of Standards and Technology (NIST), Gaithersburg, MD 20899, USA*

[2]*Graduate Institute of Applied Physics, National Taiwan University, Taipei 106, Taiwan*

[3]*Department of Physics, National Taiwan University, Taipei 106, Taiwan*

[†]These authors contributed equally to this work.

*randolph.elmquist@nist.gov and ctliang@phys.ntu.edu.tw

Abstract

We report carrier density measurements and electron-electron (*e*-*e*) interactions in monolayer epitaxial graphene grown on SiC. The temperature (*T*)-independent carrier density determined from the Shubnikov-de Haas (SdH) oscillations clearly demonstrates that the observed logarithmic temperature dependence of Hall slope in our system *must* be due to *e*-*e* interactions. Since the electron density determined from conventional SdH measurements does not depend on *e*-*e* interactions based on Kohn's theorem, SdH experiments appear to be more reliable compared with the classical Hall effect when one studies the *T* dependence of the carrier density in the low *T* regime. On the other hand, the logarithmic *T* dependence of the Hall slope $\delta R_{xy}/\delta B$ can be used to probe *e*-*e* interactions even when the conventional conductivity method is not applicable due to strong electron-phonon scattering.

Introduction

Graphene, which is a layer of carbon atoms bonded in a hexagonal lattice, has continued to attract much interest because of its importance in scientific research as well as applications in modern technologies [1, 2]. Although monolayer graphene prepared by mechanical exfoliation is of the best quality, practical use in the real world may be limited due to its available sizes [3]. Graphene grown on a copper foil by chemical vapour deposition (CVD), which can be of meter size, normally requires a transfer process [4, 5]. This could make CVD-grown graphene prone to undesirable lattice defects and contaminants. In contrast, epitaxial graphene (EG) grown on a silicon carbide (SiC) substrate can be large and does not require a transfer process, which is ideal for wafer-scale device applications [6]. To realize its potential for applications in graphene-based nanoelectronics, fundamental studies of carrier transport in epitaxial graphene on SiC are highly desirable.

At low temperatures, for a two-dimensional electron system (2DES) in the presence of a strong magnetic field perpendicular to the 2D plane, electrons are constrained to move in cyclotron orbits with discrete energy values subjected to Landau quantization. The quantum Hall effect (QHE) [3, 7], a phenomenon which is observed under Landau quantization, has been widely studied in graphene [2, 3, 7]. Characterization of electronic transport, for example in the research of graphene-based quantum Hall (QH) resistance standards [8, 9, 10], requires measurements of the carrier density since it plays a crucial role in determining the magnetic field dependence of device transport properties. Therefore, it is necessary to find a reliable method to determine the carrier density in particular at different temperatures. One method to obtain the carrier density in a 2DES or graphene is from the period of Shubnikov-de Haas (SdH) oscillations [11, 12]. A more general way to determine the carrier density is the classical Hall effect. The

Hall resistance, which shows a linear magnetic field dependence at low fields, has been widely used to calculate the carrier density of semiconductor and graphene systems [13].

Pioneering study has shown that a temperature (T)-dependent Hall slope can be mistaken as reduced dopant activation in a highly-doped silicon system [14], because at first glance the T-dependence suggests a decrease in carrier density. The underlying physics is that in a disordered 2DES at low temperatures, electron-electron (*e*-*e*) interactions are known to cause a logarithmic temperature ($\ln T$) dependence of the Hall slope and give a correction to the classical Drude conductivity [15-19]. In light of this [14-19], it is highly desirable to reliably determine the carrier density dependence of a graphene device on temperature at low T since such measurements could shed light on possible low-T charge trapping which could be detrimental to various quantum measurements and most importantly to graphene-based device stability. In this work, we show that the *T-independent* carrier density determined from the SdH oscillations clearly demonstrates that the observed $\ln T$ dependence of Hall slope in our system is the evidence of *e*-*e* interactions [17-20]. While SdH experiments are more time-consuming, they appear to be a more reliable method when one studies the T-dependence of the carrier density in any 2D system where *e*-*e* interactions may occur. In the low T regime, the SdH effect does not depend on *e*-*e* interactions in the sense that the oscillation frequencies should be robust against *e*-*e* interactions based on Kohn's theorem [21, 22]. Moreover, in studying *e*-*e* interactions, we find that measurement of the Hall slope may be applied since it is not affected by electron-phonon (*e*-*p*) scattering in the high temperature regime where conventional conductivity studies can be invalid [23].

1. Methods

Our graphene sample (Device 1) was grown on the Si face of 4H-SiC using the face-to-graphite (FTG) technique. SiC substrates were cleaned by a standard substrate cleaning procedure prior to processing. The Si-face surfaces were then placed against the polished graphite disk and orientated based on the interference pattern of the fluorescent light (Newton rings) so as to achieve a small air gap of $1-3$ μm [8]. These substrate surfaces were polished by the chemical-mechanical processed (CMP) method, resulting in uniform atomic step terraces consisting of hexagonal SiC(0001) planes. The epitaxial graphene process is controlled by annealing in a sequence of temperature ramp and dwell stages in Ar background gas at pressure about 100 kPa (1 atm) in a commercial furnace. The temperature was ramped to 1200 ℃ for 30 min and then ramped with 100 ℃/min for graphene formation at a temperature (dwell time) of 1800 ℃ for 1875 s. The typical morphology of SiC terraces of widths of 2 – 3 μm and step height of 2 – 5 nm was observed by atomic force microscopy (AFM) image analysis and the corresponding phase image shows uniform contrast as shown in Figure 1b and c. Another sample (Device 2) was grown on 6H-SiC using the same technique (ramped to 1850 ℃ for 1805 s) and was used to verify repeatability, and without further notice, data displayed in the discussion is the results of Device 1. The temperatures were measured and controlled using molybdenum-sheathed type C thermocouple probes.

A metal protective layer was first deposited on as-grown epitaxial graphene in order to prevent contamination from organic residues. The fabrication is performed by standard optical photolithography for Hall-bar configuration with size ratio $L/W = 6$ and Ti/Au contact electrodes. The protective metal layer was removed from the Hall bars using diluted aqua regia before measurement [24], which produces chemical doping by molecular adsorbates [for example, refer to Journal of Catalysis 323 (2015),

Nanotechnology 26 (2015) 445702 (7pp) 10 – 18, Nanotechnology 27 (2016) 072502 (4pp)]. The optical image of graphene Hall bar is shown in Figure 1a. Four-terminal longitudinal resistivity ρ_{xx} and Hall resistance R_{xy} were measured using standard AC lock-in techniques. Similar results obtained on Device 2 are described in Supplementary Information.

2. Results and Discussions

Figure 2 shows the Hall resistance data of monolayer EG sample at various temperatures. Negative magnetoresistance can be ascribed to weak localization (WL) [25, 26]. An emergent quantum Hall step of value $R_{xy} \approx h/(6e^2)$ corresponding to the $\nu = 6$ QH state is observed at $B > 6$ T. We plot the Hall slope $R_H = \delta R_{xy}/\delta B$ as a function of temperature in the inset of Figure 2. The data reveal a decrease of the Hall slope with increasing temperature. The carrier density, which is often obtained from the measured Hall slope $R_H \equiv B/(ne)$, is plotted as shown by n_{H} in Figure 4. To determine the carrier density independently, we can also calculate from the SdH oscillations. Figure 3 shows the longitudinal resistivity ρ_{xx} as a function of B at various temperatures. Prominent SdH oscillations are present at low temperatures with minima at filling factors $\nu = 10$ and $\nu = 6$, demonstrating that we have a monolayer graphene device. Since the minima in B of the SdH oscillations do not shift at different temperatures as shown in the inset of Figure 3, the carrier density is T-independent and is calculated to have the value $n_{SdH} = 1.140\times10^{12}$ cm^{-2} from $n = \nu Be/h$, as shown in Figure 4. The peak positions at around $B = 6$ T in Figure 3 are shown to move with increasing temperature as a feature of scaling behavior of standard quantum Hall theory [27].

In Figure 4, the carrier densities calculated from two methods show different values,

which can also be seen in a traditional $Al_xGa_{1-x}N/GaN$ heterostructure device [28]. Here, we observed that the carrier density n_{H} obtained from the measured Hall slope appears to increase with increasing temperature. However, the fact that the minima in *B* of the SdH oscillations do not shift with temperature makes evident that the carrier density remained unchanged at different temperatures [21, 22]. The data of a Si δ-doped GaAs quantum well sample with additional modulation-doping [29] is shown in Figure 10 of the supplementary information to illustrate that we did observe that the minima in *B* of the SdH oscillations shift with temperature, which can only be ascribed to the change in the carrier density due to the carriers released by the dopants with increasing temperature. Therefore, the *T*-independent carrier density n_{SdH} in our graphene sample demonstrates that the change of the Hall slope *cannot* be due to the change in the carrier density at different temperatures.

In order to understand the physical origin of the *T* dependence of R_H, we plot the experimental R_H as a function of temperature on a semi-logarithmic scale in Figure 5 and we observe that R_H varies with ln *T*. For a disordered 2DES, *e*-*e* interactions give a correction to the longitudinal conductivity which is given by [20]

$$\delta\sigma_{ee} = K_{ee}G_0 \ln\frac{kT\tau}{\hbar}, \qquad (1)$$

where τ is the transport relaxation time, $G_0 = e^2/\pi h$, and K_{ee} is a parameter dependent on the screened Coulomb interaction. Since *e*-*e* interactions do not affect the Hall conductivity σ_{xy} [15, 16], this term gives a ln*T* dependence to σ_{xx} and to both the resistivities ρ_{xx} and ρ_{xy}. The Hall slope including the *e*-*e* interactions correction δR_H via tensor inversion can be written as

$$R_H = R_H^0 + \delta R_H = \frac{\rho_{xy}}{B} = \frac{\sigma_{xy}/B}{(\sigma_0 + \delta\sigma_{ee})^2 + \sigma_{xy}^2}, \qquad (2)$$

where $\sigma_{xx} = \sigma_0 + \delta\sigma_{ee}$ with WL corrections neglected since WL does not produce a

correction in R_H in the commonly assumed first order perturbation, σ_0 is the Drude conductivity, $\delta\sigma_{ee}$ is the correction given by Eq. (1), and R_H^0 is the classical value of R_H. The red curve in Figure 5 is then plotted using Eq. (2) where σ_{xx}(30 K, 0 T) and σ_{xy}(30 K) were used to approximate the value of σ_0 and σ_{xy}, respectively, and $K_{ee} = 0.71$, which is determined by optimizing the elimination of the *e-e* interactions correction from the resistivity tensor [20, 30]. The good fit to our data demonstrates that the observed ln$T$ dependence in R_H can be ascribed to *e-e* interactions. In addition, for small $\delta\sigma_{ee}/\sigma_0$, Eq. (2) can further reduce to the common expression

$$\frac{\delta R_H}{R_H^0} = -2\frac{\delta\sigma_{ee}}{\sigma_0}, \qquad (3)$$

which provides an alternative method for characterizing *e-e* interactions through the T dependence of R_H. The measured R_H shows a ln$T$ dependence for $1.5\ \text{K} \leq T \leq 30\ \text{K}$ in the lower inset of Figure 5, supporting the evidence of *e-e* interactions at low T in our graphene device [17-20]. By replacing R_H^0 and σ_0 with R_H(30 K) and σ_{xy}(30 K) in Eq. (3), the interaction correction to the zero field conductivity can be extracted and also shows the expected ln$T$ dependence, as seen in the top inset of Figure 5.

For further investigation, we probe the *e-e* interactions by studying the T dependence of the longitudinal conductivity. The measured conductivity at low temperatures can be described by $\sigma_{xx} = \sigma_0 + \delta\sigma_{WL} + \delta\sigma_{ee}$ [18]. Since the Drude conductivity σ_0 is T-independent at low temperatures [23, 25], we can also study the *e-e* interactions effect by subtracting the WL correction term. As shown in Figure 6, by fitting the converted magnetoconductivity in the low magnetic field regime to the model for monolayer graphene derived by McCann *et al* [31], we can calculate the WL contribution [25]. Figure 7 shows the longitudinal conductivity σ_{xx} with and without subtraction of the

WL correction term as a function of temperature at $B = 0$. We can see that after subtraction of the WL contribution, σ_{xx} decreases with increasing temperature for $T > 7$ K as a result of enhanced *e*-*p* scattering [32, 33]. In this case, by taking the data at $T = 7$ K as a reference point, we can only study the *e*-*e* interactions from 1.5 K to 7 K. The Hall slope, which remains its linear trend against ln$T$ up to at least $T = 30$ K, is not affected by the *e*-*p* scattering over a wider temperature range, hence the T dependence of R_H provides a useful tool for investigation of *e*-*e* interactions in this high temperature regime.

We have shown that the ln$T$ dependence of the Hall slope caused by the *e*-*e* interactions can decrease the Hall slope and hence results in the seemly observed T-dependent carrier density. Therefore, SdH measurements, which do not depend on *e*-*e* interactions [21, 22], appear to be a more reliable method to determine the carrier density in the low T regime. Furthermore, for doped Si-based samples with low mobilities [14], it is not possible to determine the carrier density from SdH oscillations measurements since SdH oscillations cannot be observed with experimentally achievable magnetic fields. In contrast to our graphene samples with higher mobilities, SdH oscillations appear at lower fields, providing us an alternative and reliable method for the determination of the carrier density independently. In strongly disordered graphene, although a T-independent point in R_{xx} over a wide range of temperature does suggest that the carrier density is temperature-independent [30, 34], the lack of SdH oscillations did not allow us to probe the carrier density [30].

It has been reported that the orientation of Hall bar with respect to the terraces on SiC and patches of bilayer graphene forming at step edges are responsible for an anisotropy in the quantum Hall effect [35-37]. As shown in Figure 1a, in our graphene Hall bar,

the current is at an angle of about 9° with respect to the terraces and therefore the conduction path crosses many surface steps. It has been shown that when devices are placed on shallow steps, the direction of the terraces with respect to the Hall bar makes little difference, if any, to the transport properties, but bilayer domains do lead to anisotropic transport [37]. Since our SdH data show well-defined resistance minima whose value decrease with increasing magnetic field and we do not observe positive magnetoresistance in the high magnetic field regime [36], and because our sample has relatively low terrace step height (2 – 5 nm),it is likely that bilayer graphene is mostly absent at step edges, resulting in homogeneous transport. We thus believe that the direction of current flow relative to that of the terrace steps may not affect the determination of carrier density from SdH oscillations as well as the *T* dependence of the Hall slope in our wide Hall bars. Nevertheless, by fabricating a L-shape Hall bar [38] aligning with the terrace on SiC that allows transport parallel and perpendicular to the terraces to be probed within the same graphene device, one will be able to obtain a thorough understanding of the low-temperature dependence of the carrier density determined by both Hall and SdH measurements, an interesting issue that warrants future investigation.

The *T*-independence of the carrier density in our system is evidence that the charge trapping model in epitaxial graphene on SiC is not applicable in the low temperature regime [39, 40]. It is also worth mentioning that at high temperatures, from Device 2 (see Figure 5 in supplementary information) the Hall slope deviates from the red solid line and we cannot simply ascribe this abrupt change to the *e*-*e* interactions. Neither can we attribute this phenomenon simply to the charge trapping effect since our data cannot be fitted to the Arrhenius-type equation [39, 40]. It is possible that in our device the carrier density does increase in the high temperature regime.

3. Conclusions

We have reported the *e-e* interactions and carrier density measurements in monolayer epitaxial graphene. High mobilities and low carrier densities in epitaxial graphene samples allow us to observe the SdH oscillations at practically achievable magnetic fields. Our results show that the *T*-independent carrier density determined from the SdH oscillations clearly demonstrates that the observed ln*T* dependence of Hall slope in our system must be due to *e-e* interactions. On the other hand, the ln*T* dependence of the Hall slope can be used to probe *e-e* interactions even when the conventional conductivity method is not applicable due to strong *e-p* scattering at high temperatures. SdH experiments, which do not depend on *e-e* interactions, are therefore shown to be a more reliable method comparable to the classical Hall effect when one studies the *T* dependence of the carrier density in the low *T* regime.

Acknowledgements

We acknowledge the support from the Ministry of Science and Technology, Taiwan (Grant numbers: MOST 104-2811-M-002-250 and MOST 105-2119-M-002-048-MY3). We thank Prof. David Goldhaber-Gordon for useful discussions.

References

[1] Geim A K and Novoselov K S 2007 The rise of graphene *Nat. Mater.* **6** 183-191

[2] Novoselov K S *et al* 2005 Two-dimensional gas of massless Dirac fermions in graphene *Nature* **438** 197-200

[3] Zhang Y, Tan Y-W, Stormer H L and Kim P 2005 Experimental observation of the quantum Hall effect and Berry's phase in graphene *Nature* **438** 201-204

[4] Hofmann M, Hsieh Y-P, Hsu A L and Kong J 2014 Scalable, flexible and high

resolution patterning of CVD graphene *Nanoscale* **6** 289-292

[5] Obraztsov A N 2009 Chemical vapour deposition: Making graphene on a large scale *Nat. Nanotechnol.* **4** 212-213

[6] Lin Y-M *et al* 2011 Wafer-Scale graphene integrated circuit *Science* **332** 1294-1297

[7] Zhang Y *et al* 2006 Landau-level splitting in graphene in high magnetic fields *Phys. Rev. Lett.* **96** 136806

[8] Real M A *et al* 2013 Graphene epitaxial growth on SiC(0001) for resistance standards *IEEE Trans. Instrum. Meas.* **62** 1454-1460

[9] Lafont F *et al* 2015 Quantum Hall resistance standards from graphene grown by chemical vapour deposition on silicon carbide *Nat. Commun.* **6** 6806

[10] Janssen T J B M *et al* 2015 Operation of graphene quantum Hall resistance standard in a cryogen-free table-top system *2D Mater.* **2** 035015

[11] Isihara A and Smrcka L 1986 Density and magnetic field dependences of the conductivity of two-dimensional electron systems *J. Phys. C* **19** 6777-6789

[12] Tiras E *et al* 2013 S Effective mass of electron in monolayer graphene: Electron-phonon interaction *J. Appl. Phys.* **113** 043708

[13] Peres N M R, Lopes dos Santos J M B and Stauber T 2007 Phenomenological study of the electronic transport coefficients of graphene *Phys. Rev. B* **76** 073412

[14] Goh K E J, Simmons M Y and Hamilton A R 2007 Use of low-temperature Hall effect to measure dopant activation: Role of electron-electron interactions *Phys. Rev. B* **76** 193305

[15] Altshuler B L *et al* 1980 Magnetoresistance and Hall effect in a disordered two-dimensional electron gas *Phys. Rev. B* **22** 5142

[16] Altshuler B L, Aronov A G, and Lee P A 1980 Interaction effects in disordered Fermi systems in two dimensions *Phys. Rev. Lett.* **44** 1288

[17] Uren M J, Davies R A, Kaveh M and Pepper M 1981 Logarithmic corrections to

two-dimensional transport in silicon inversion layers *J. Phys. C* **14** 5737-5762

[18] Lee P A and Ramakrishnan T V 1985 Disordered electronic systems *Rev. Mod. Phys.* **57** 287-337

[19] Simmons M Y *et al* 2000 Weak localization, hole-hole interactions, and the "metal"-insulator transition in two dimensions *Phys. Rev. Lett.* **84** 2489-2492

[20] Goh K E J, Simmons M Y and Hamilton A R 2008 Electron-electron interactions in highly disordered two-dimensional systems *Phys. Rev. B* **77** 235410

[21] Kohn W 1961 Cyclotron resonance and de Haas-van Alphen oscillations of an interacting electron gas *Phys. Rev.* **123** 1242

[22] Goswami P, Jia X and Chakravarty S 2008 Quantum oscillations in graphene in the presence of disorder and interactions *Phys. Rev. B* **78** 245406

[23] Liu C-I *et al* 2016 Probing electron–electron interactions in multilayer epitaxial graphene grown on SiC using temperature-dependent Hall slope *Solid State Commun.* **236** 41-44

[24] Yang Y *et al* 2015 Low carrier density epitaxial graphene devices on SiC *Small* **11** 90-95

[25] Liang C-T *et al* 1994 Weak localization and electron-electron interactions in a two-dimensional grid lateral surface superlattice *Phys. Rev. B* **49** 8518-8521

[26] Zion E *et al* 2015 Localization of charge carriers in monolayer graphene gradually disordered by ion irradiation *Graphene* **4** 45-53

[27] Huang C F *et al* 2002 Insulator-quantum Hall conductor transitions at low magnetic field *Phys. Rev. B* **65** 045303

[28] Lo I *et al* 2002 Spin splitting in modulation-doped $Al_xGa_{1-x}N$/GaN heterostructures *Phys. Rev. B* **65** 161306

[29] Chen K Y *et al* 2008 Probing Landau quantization with the presence of insulator–quantum Hall transition in a GaAs two-dimensional electron system *J. Phys*

Condens. Matter **20** 295223

[30] Huang L I *et al* 2016 Insulator-quantum Hall transition in monolayer epitaxial graphene *RSC Adv.* **6** 71977

[31] McCann E *et al* 2006 Weak-localization magnetoresistance and valley symmetry in graphene *Phys. Rev. Lett.* **97** 146805

[32] Hwang E H and Das Sarma S 2008 Acoustic phonon scattering limited carrier mobility in two-dimensional extrinsic graphene *Phys. Rev. B* **77** 115449

[33] Efetov D K and Kim P 2010 Controlling electron-phonon interactions in graphene at ultrahigh carrier densities *Phys. Rev. Lett.* **105** 256805

[34] Liu F-H *et al* 2013 Dirac fermion heating, current scaling, and direct insulator-quantum Hall transition in multilayer epitaxial graphene *Nanoscale Res. Lett.* **8**, 360

[35] Giannazzo F *et al* 2012 Electronic transport at monolayer-bilayer junctions in epitaxial graphene on SiC *Phys. Rev. B* **86**, 235422

[36] Schumann T *et al* 2012 Anisotropic quantum Hall effect in epitaxial graphene on stepped SiC surfaces *Phys. Rev. B* **85**, 235402

[37] Yager T *et al* 2013 Express optical analysis of epitaxial graphene on SiC: impact of morphology on quantum transport *Nano Lett.* **13**, 421

[38] Papadakis S J *et al* 2000 Anisotropic magnetoresistance of two-dimensional holes in GaAs *Phys. Rev. Lett.* 84 5592-5595

[39] Farmer D B *et al* 2010 Charge trapping and scattering in epitaxial graphene *Phys. Rev. B* **84** 205417

[40] Liu C-I *et al* 2016 Charge trapping in monolayer and multilayer epitaxial graphene *Journal of Nanomaterials* **2016** 7372812

FIGURE CAPTIONS

Figure 1: (a) Optical image of graphene Hall bar (marked by dashed yellow lines). (b)

AFM height image. The inset shows height profile along the line indicated. (c) AFM phase image corresponding to height image.

Figure 2: Hall resistance data of various temperatures. The inset shows Hall slope (R_H) as a function of temperature.

Figure 3: Longitudinal resistivity ρ_{xx} as a function of magnetic field at various temperatures. The inset shows the minima in magnetic field of the SdH oscillations against temperature at $\nu = 10$ and $\nu = 6$.

Figure 4: The carrier density determined from the SdH oscillations n_{SdH} and from the measured Hall slope n_{H} as a function of temperature.

Figure 5: R_H as a function of temperature on a semilogarithmic scale. The red curve fits to the data according to Equation 2. The lower inset shows R_H as a function of ln$T$. There is a good linear fit (red solid line) for 1.5 K $\leq T \leq$ 30 K. The top inset shows *e-e* interactions correction term $\delta\sigma_{ee}$ as a function of ln$T$.

Figure 6: $\Delta\sigma_{xx} = \sigma_{xx}(B) - \sigma_{xx}(B = 0)$ at various temperatures. The red curves correspond to the fits to the model for monolayer graphene in the low magnetic field regime at different temperatures 1.5 K $\leq T \leq$ 30 K.

Figure 7: Longitudinal conductivity with and without subtraction of the WL term as a function of temperature on a semi-logarithmic scale at $B = 0$.

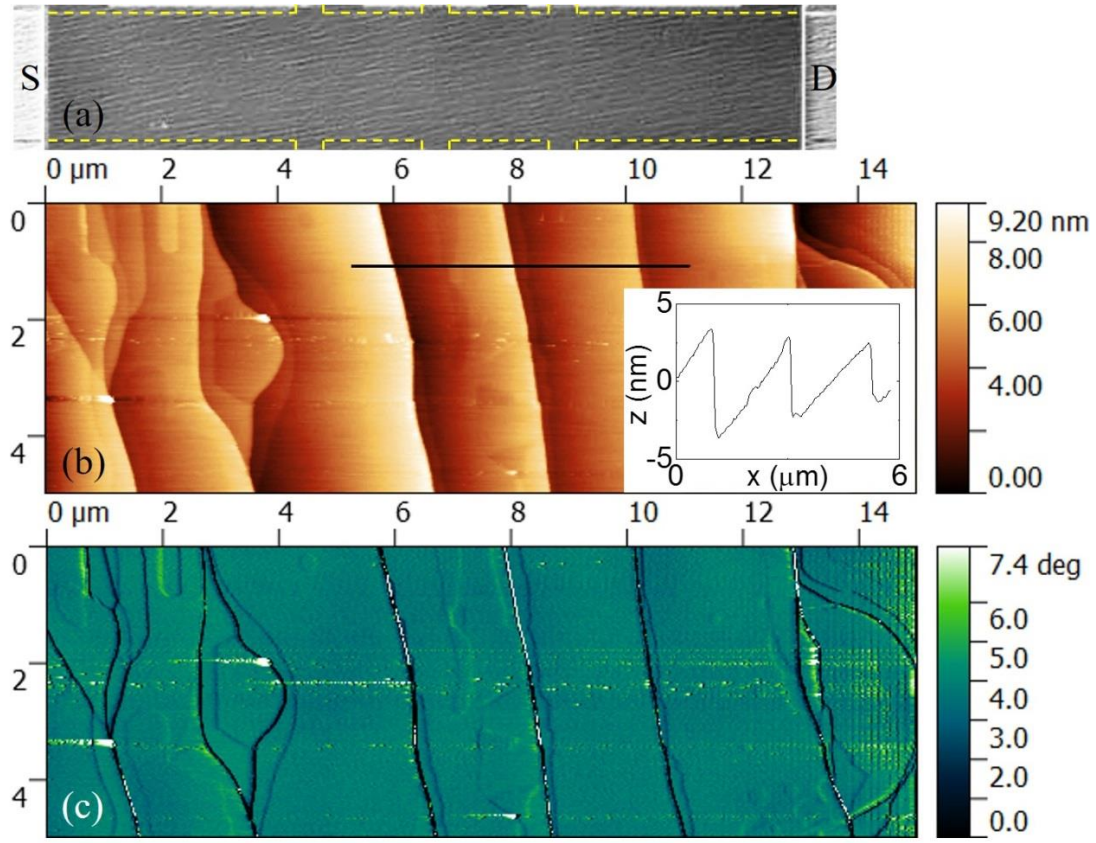

Figure 1

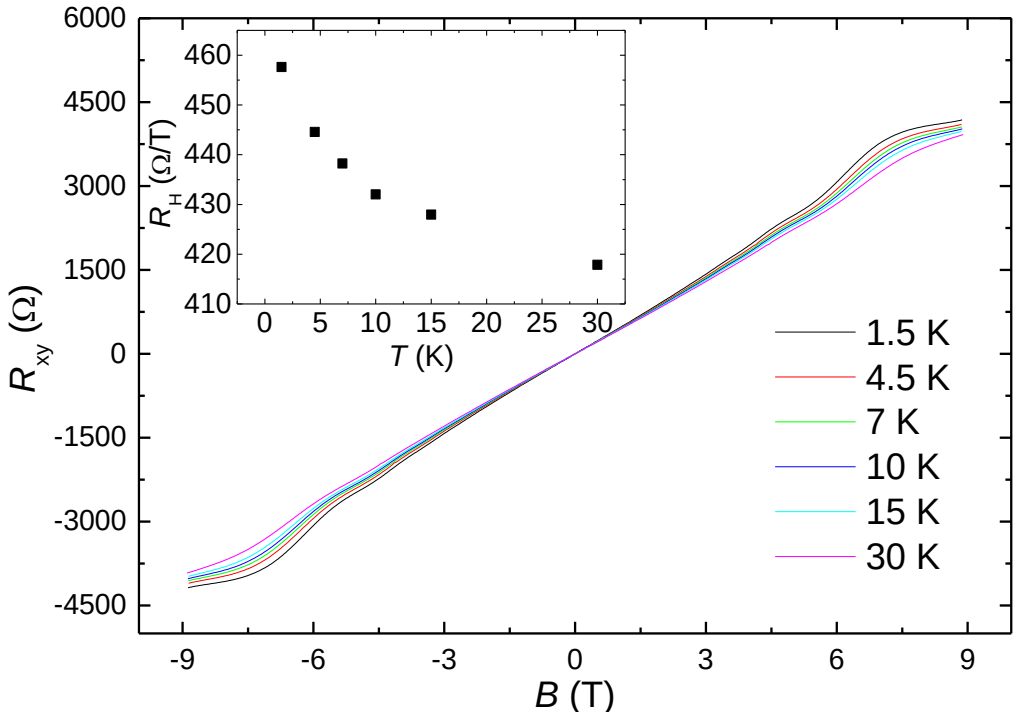

Figure 2

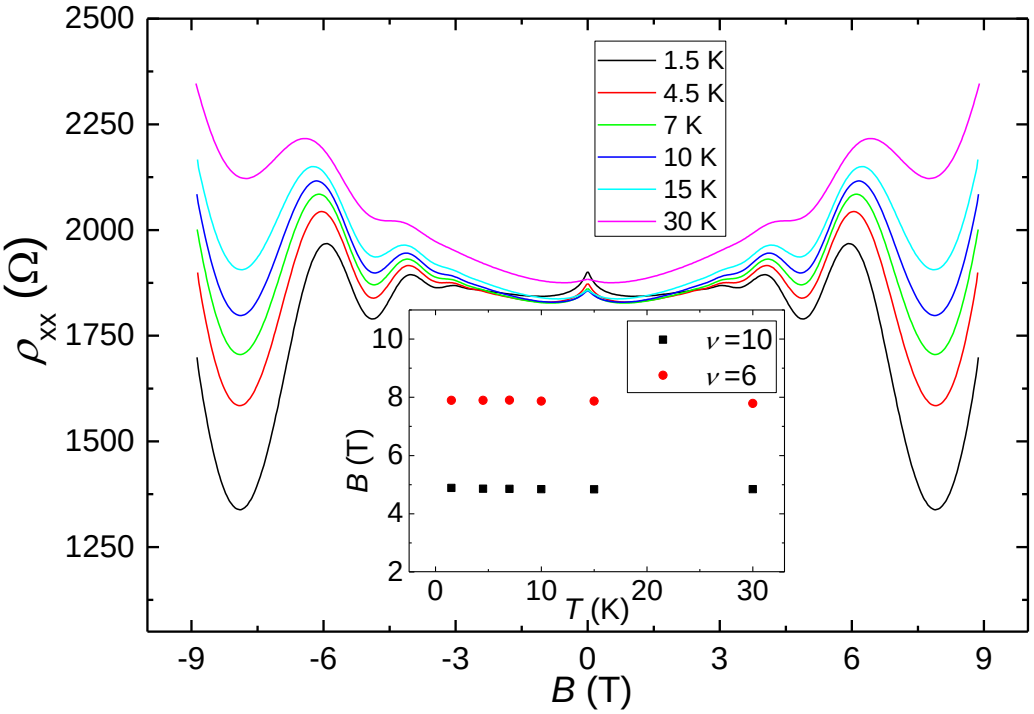

Figure 3

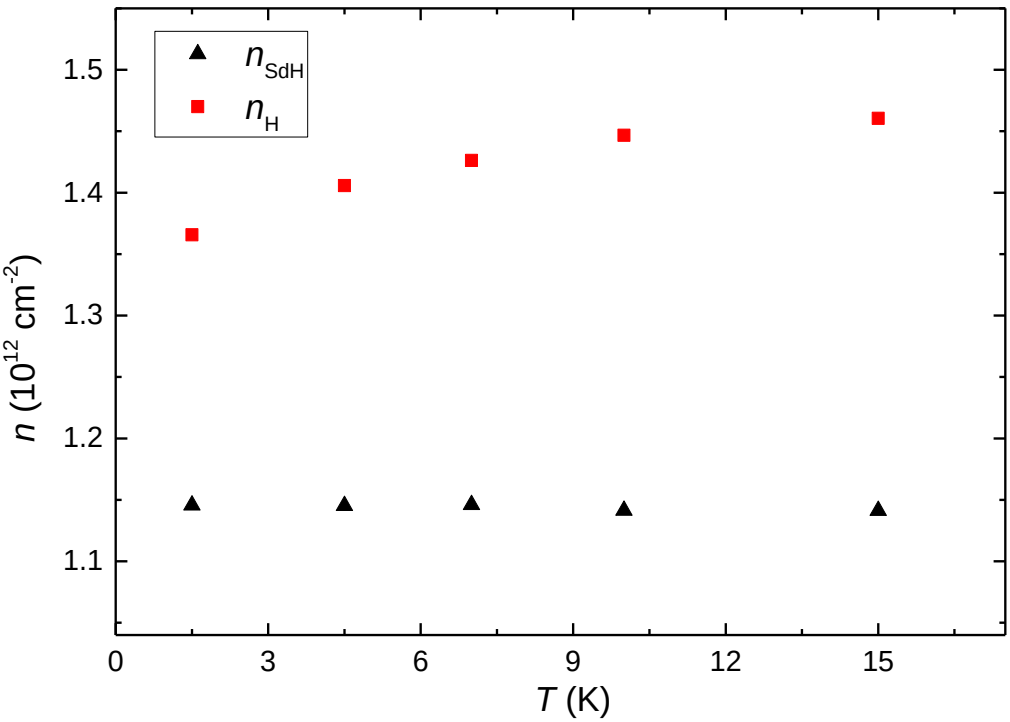

Figure 4

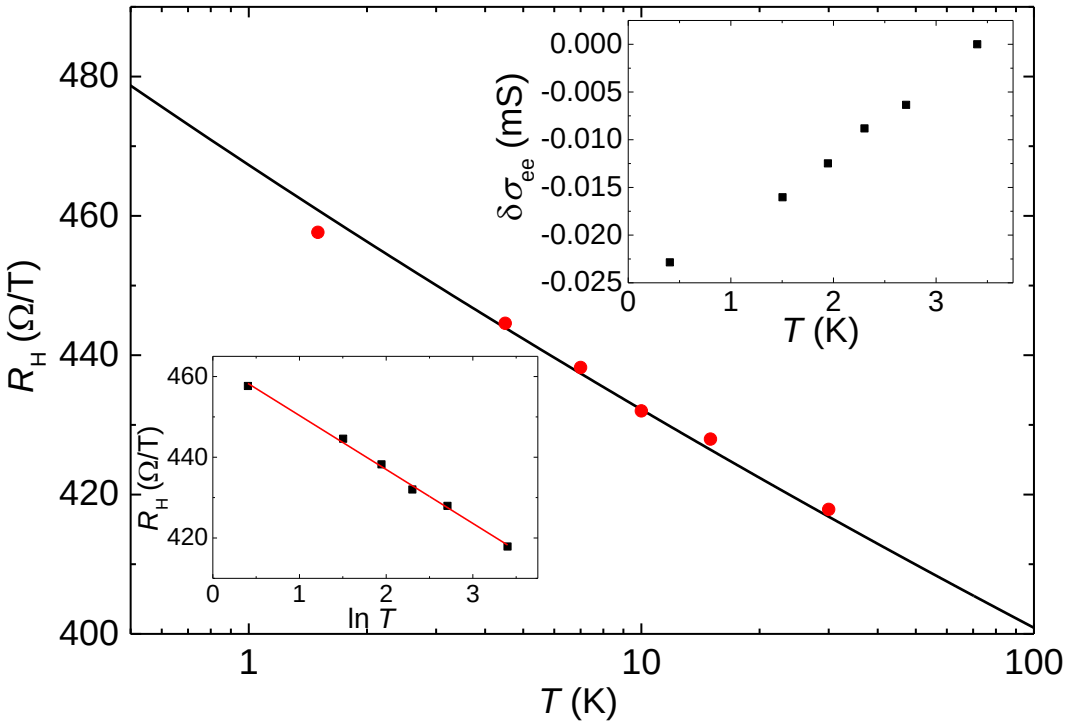

Figure 5

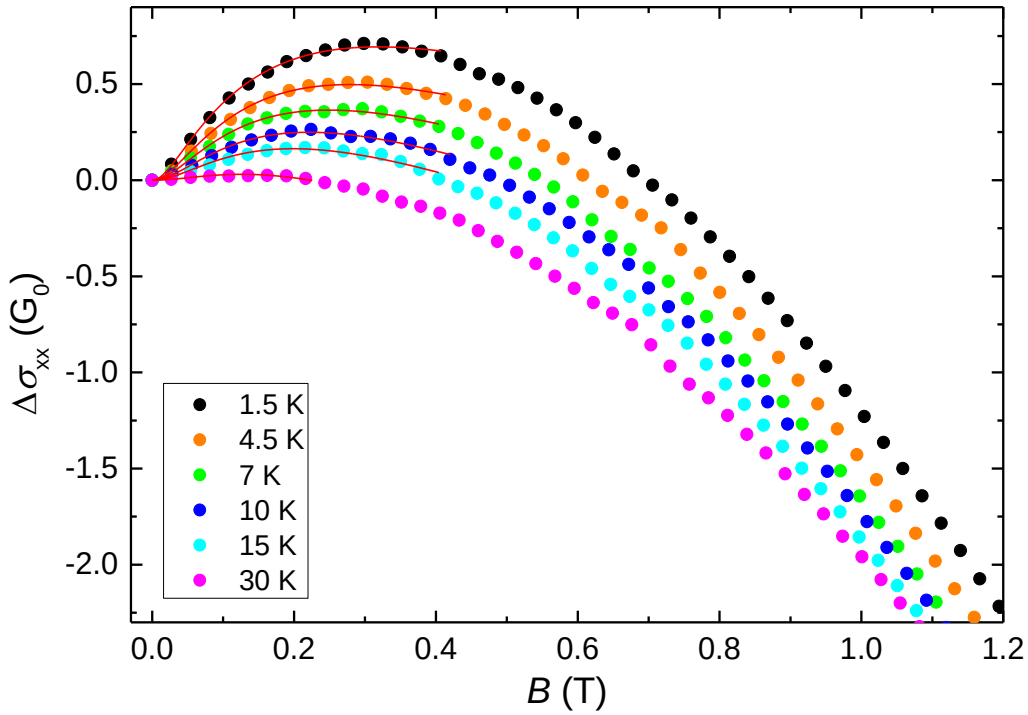

Figure 6

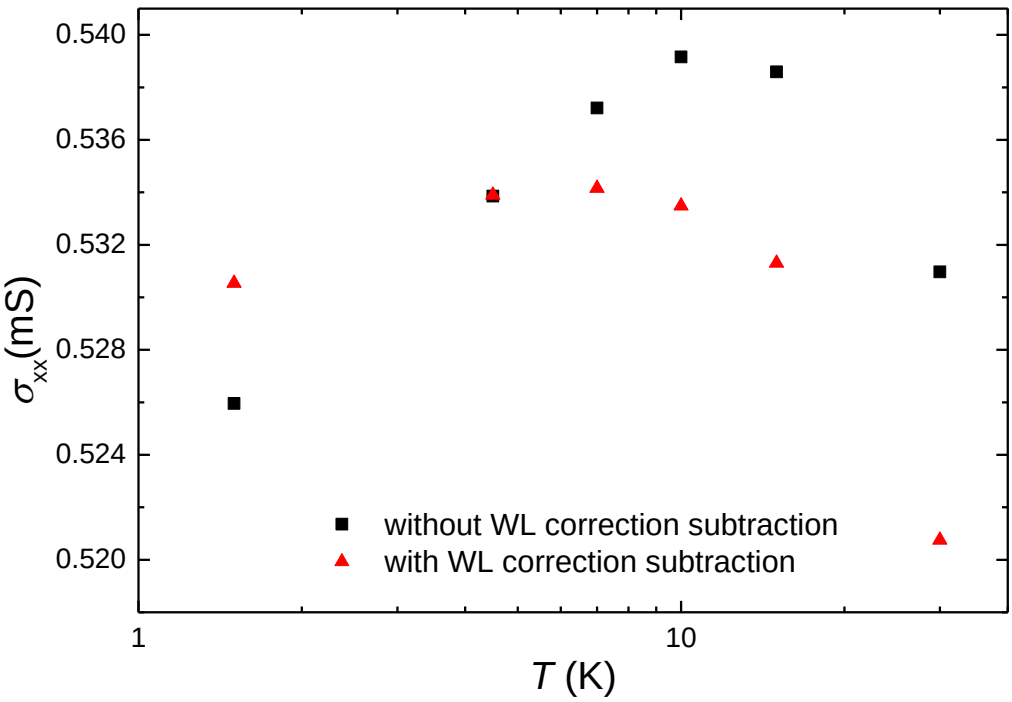
0.540
0.536
0.532
0.528
0.524
0.520
σ_{xx} (mS)
1
10
T (K)
without WL correction subtraction
with WL correction subtraction

Figure 7

Supplementary Information

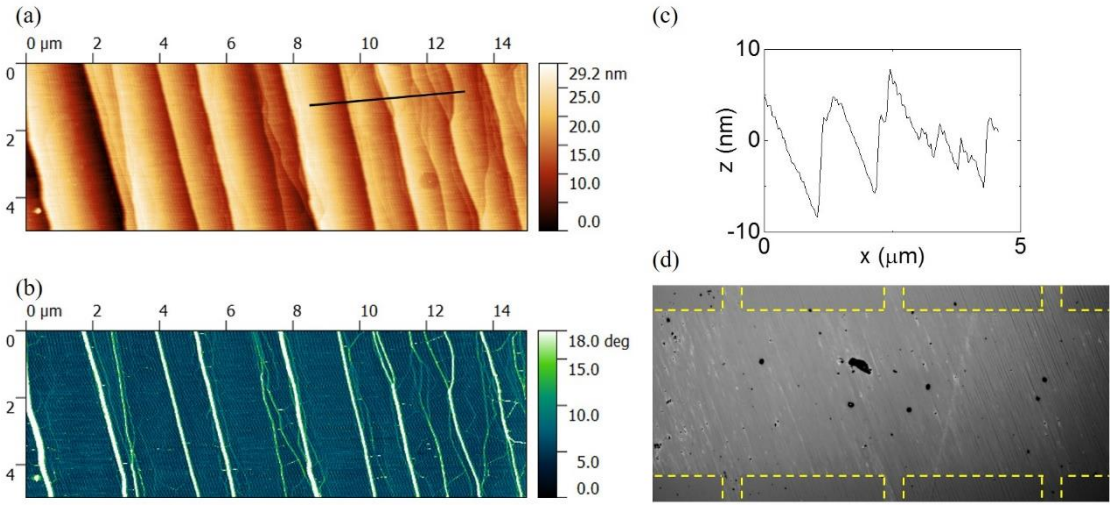

Fig. 1 (Device 2) (a)AFM height image. (b) AFM and phase images corresponding to height image. (c) Height profile along the line indicated in (a). (d) Optical image of graphene Hall bar (marked by dashed yellow line).

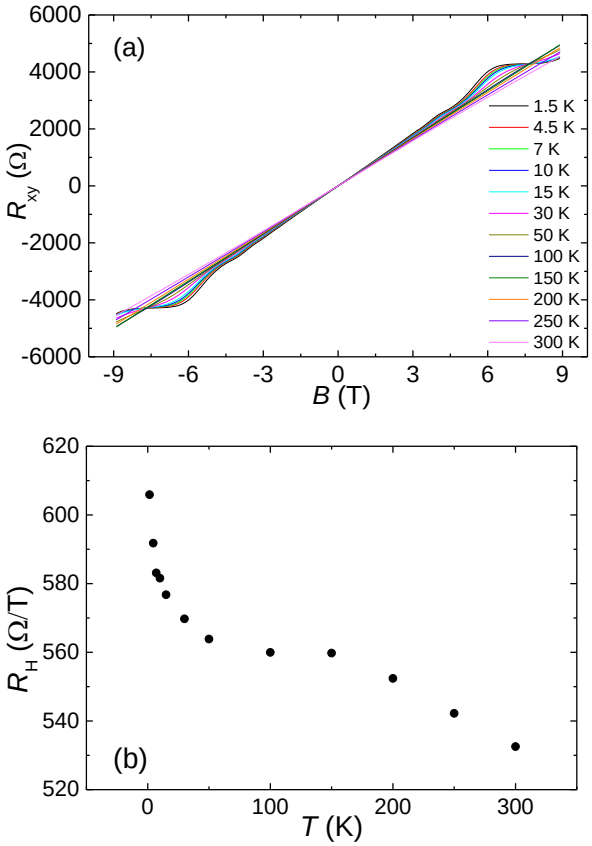

Fig. 2 (Device 2) (a) Hall resistance data various temperature. (b) Hall slope (R_H) as a function of T.

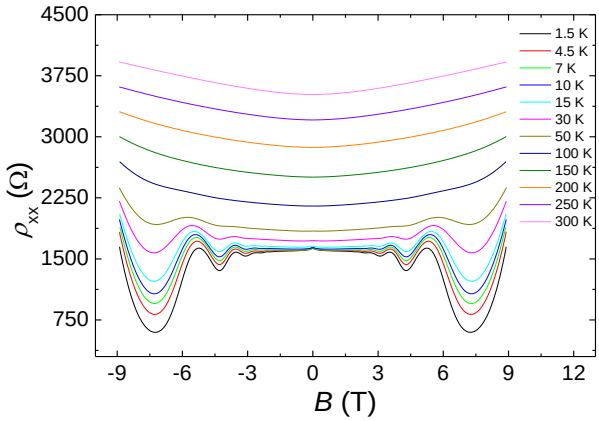

Fig.3 (Device 2) Longitudinal resistivity ρ_{xx} as a function of magnetic field at various temperatures.

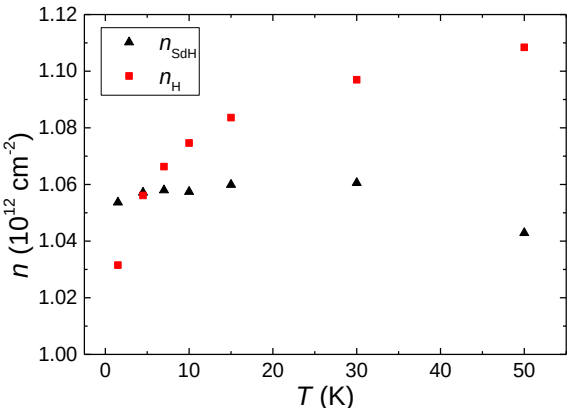

Fig. 4 (Device 2) n_{SdH} and n_{H} as a function of temperature.

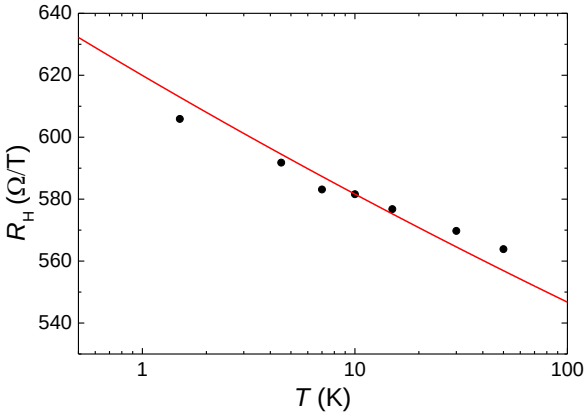

Fig. 5 (Device 2) R_H as a function of temperature on a semilogarithmic scale. The red curve fits to the data using Equation 2.

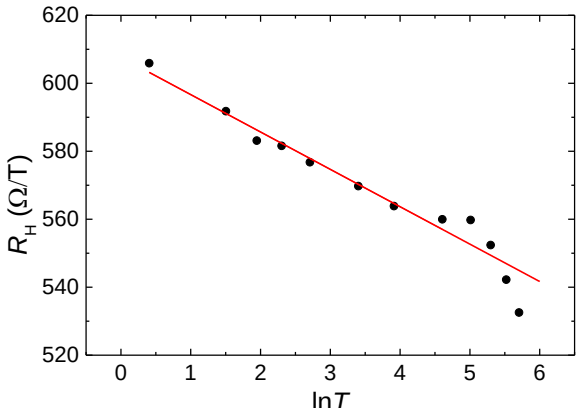

Fig. 6 (Device 2) R_H as a function of ln$T$. There is a good linear fit (red solid line) for $1.5\ \text{K} \leq T \leq 50\ \text{K}$.

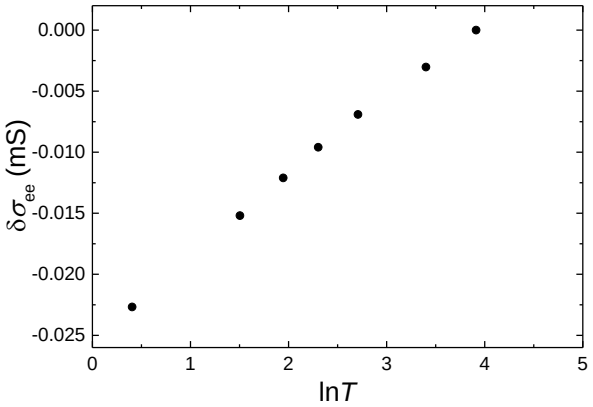

Fig. 7 (Device 2) *e-e* interactions correction term as a function of ln *T*.

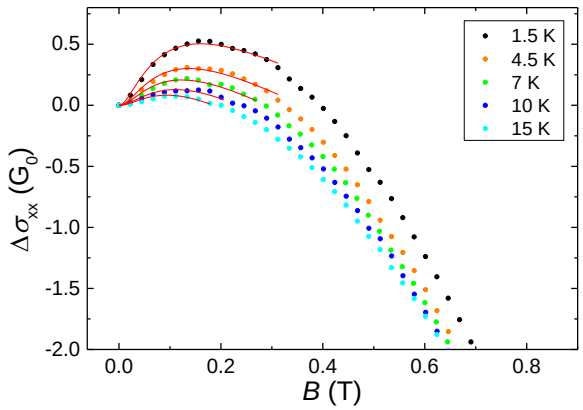

Fig. 8 (Device 2) $\Delta\sigma_{xx} = \sigma_{xx}(B) - \sigma_{xx}(B = 0)$ at various temperatures. The red curve correspond to the fits to the model for monolayer graphene in the low magnetic field regime at different temperatures $1.5\ \text{K} \leq T \leq 15\ \text{K}$.

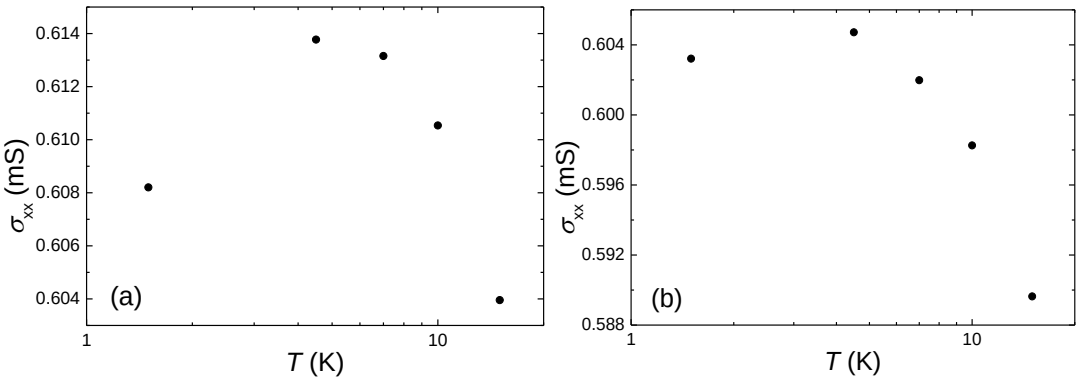

Fig.9 (Device 2) (a) Longitudinal conductivity as a function of temperature on a semi-logarithmic scale at $B = 0$. (b) Longitudinal conductivity after subtraction of the WL term as a function of temperature on a semi-logarithmic scale at $B = 0$.

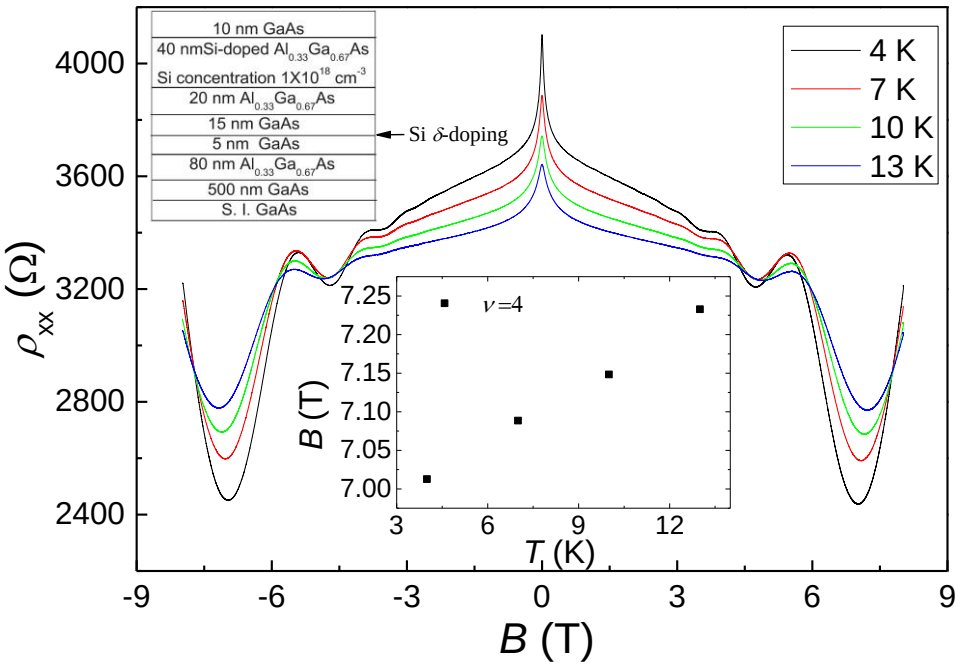

Fig. 10 (Si δ-doped GaAs quantum well sample with additional modulation doping) Longitudinal resistivity ρ_{xx} as a function of magnetic field at various temperatures. The top inset shows the sample structure. The lower inset shows the minima in magnetic field of the SdH oscillations against temperature at ν=4.